THE JOURNAL OF PHYSICAL CHEMISTRY C

ARTICLE

pubs.acs.org/JPCC

Ultrafast Relaxation of the Poly(3-hexylthiophene) Emission Spectrum

Natalie Banerji,[†] Sarah Cowan,[†] Eric Vauthey,[‡] and Alan J. Heeger*[,†]

[†]Center for Polymers and Organic Solids, University of California at Santa Barbara, Santa Barbara, California 93106-5090, United States

[‡]Department of Physical Chemistry, University of Geneva, 30 Quai Ernest-Ansermet, CH-1211 Geneva 4, Switzerland

ABSTRACT: The femtosecond-resolved evolution of the emission spectrum of the important conjugated polymer poly(3-hexylthiophene) (P3HT) is presented. Detailed fluorescence up-conversion spectroscopy was performed on P3HT solid-state films and on P3HT in chlorobenzene solution. Two excitation wavelengths and several emission wavelengths, covering the entire fluorescence spectrum, were used. The data were complemented by polarization-sensitive measurements. Our global analysis allowed a reconstruction of the time-resolved emission spectra with 200 fs temporal resolution, so that spectral changes due to the early relaxation processes following $\pi-\pi^*$ interband absorption in the pristine polymer could be comprehensively characterized. Absorption occurs in isolated polymer chains in solution and in the solid state (including interchain interactions) for the film. In both cases, we find evidence of delocalization of the electrons and holes formed in the energy bands directly after photoexcitation with excess energy. This is followed by ultrafast (~100 fs) self-localization of the primary photoexcitation and by relatively slow exciton formation (~1 ps). Further relaxation occurs with time constants ranging from hundreds of femtoseconds to tens of picoseconds, due to exciton hopping to sites with lower energy and to a slow conformational planarization of the polymer backbone. Depolarization, a spectral red shift, and important changes in the vibronic structure are observed as a consequence of this relaxation. Finally, relaxed intrachain and interchain singlet excitons are formed in solution and film, respectively, on a 100−200 ps time scale. They decay with a ~500 ps time constant, by intersystem crossing in solution and by nonradiative recombination in the film. Our results are consistent with and strongly support the conclusions we obtained from a similar time-resolved fluorescence study of the polymer PCDTBT (*J. Am. Chem. Soc.* **2010**, *132*, 17459): ultrafast charge separation in polymer:fullerene blends seems to occur before localization of the primary excitation to form a bound exciton.

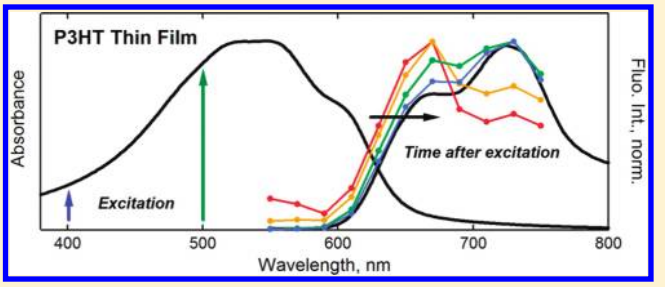

1. INTRODUCTION

The optoelectronic properties of conjugated polymers combined with "plastic" mechanical behavior and solution processability make them highly interesting materials with applications in organic electronics.[1−5] In bulk heterojunction (BHJ) solar cells, an electron-donating conjugated polymer is blended with a fullerene electron acceptor, such as [6,6]-phenyl C_{60} butyric acid methyl ester (PCBM).[6−12] This yields a nanoscale morphology in the thin film active layer with a high donor−acceptor interfacial area for efficient photoinduced charge separation and with phase-separated fullerene and polymer networks for charge transport to the electrodes. Regioregular poly(3-hexylthiophene), abbreviated as P3HT throughout the text, has been thoroughly investigated and is considered a state of the art material. High power conversion efficiencies, around 5%, can be obtained in thermally annealed P3HT:PCBM devices.[8,13−15]

A key to optoelectronic device functioning is the interaction of the conjugated polymer with light. Numerous steady-state and time-resolved spectroscopic studies have been conducted in pristine P3HT and P3HT:PCBM blends in order to understand the nature and evolution of neutral and charged excitations,[16−56] but many aspects of the photophysics remain unclear. This is explained by the general complexity of light-induced processes in conjugated polymers,[57−60] as well as by additional complications that arise because of the strong interchain interactions in the partially microcrystalline film morphology of P3HT. Indeed, the P3HT chains in thin films π-stack into two-dimensional lamellae sheets perpendicular to the substrate with interchain distances of only 3.8 Å.[61] Amorphous conjugated polymers can be treated as one-dimensional semiconductors where excitations are localized on single polymer chains.[62] On the other hand, it has been shown in P3HT films that both neutral excitations[17,26,29,36,40,42,43,45,48,54] and charged polarons[20,46,49−51] are at least partially delocalized over neighboring polymer chains and become quasi-two-dimensional interchain species. This infers unique properties to the polymer, such as a relatively high charge carrier mobility [approximately 0.1 $cm^2/(V\ s)$][61] and a high yield, up to 30%, of photogenerated charge carriers in pristine P3HT films.[38]

We report here an ultrafast emission study of pristine P3HT in spin-cast thin films and dilute chlorobenzene (CB) solution, as measured by femtosecond-resolved fluorescence up-conversion (FU). This technique selectively probes neutral singlet excitations and is not concerned with charged polarons or triplet states, in contrast to transient absorption spectroscopy. Data recorded

Received: December 15, 2010
Revised: March 17, 2011
Published: April 22, 2011

over several emission wavelengths are compared for two excitation wavelengths and are supplemented by fluorescence polarization measurements. Such a comprehensive and systematic approach has not been used in previously reported time-resolved emission investigations of P3HT.[16,17,21,23,24,37,44,54] Furthermore, those studies obtained either single-wavelength FU dynamics with a ~200 fs time resolution or entire emission spectra with a lower time resolution of several picoseconds typical for streak cameras. Here, we use the FU dynamics obtained at many emission wavelengths to reconstruct the emission spectra with a ~200 fs time resolution. This reveals important spectral changes directly following light absorption in P3HT, in particular where the relative intensity of the vibronic transitions is concerned. Detailed information about the early relaxation dynamics of the primary photoexcitations in the pristine polymer can be retrieved. Those relaxation processes are important to understand, since they occur on a similar time scale as charge separation in P3HT:PCBM blends.[18,32] Therefore, they are directly relevant to the functioning of BHJ solar cells.

2. EXPERIMENTAL METHODS

2.1. Samples. Regioregular poly(3-hexylthiophene) was synthesized by Rieke Metals, Inc., according to the Rieke method (M_n = 33.4 kDa, M_w = 79.9 kDa, PDI = 2.4, regioregularity = 92.1%). For thin film fabrication, a 10 mg/mL solution of P3HT in chlorobenzene (Sigma-Aldrich, anhydrous, 99.8%) was spin-cast on a circular quartz substrate (Saint-Gobain Spectrosil 2000) at 3500 rpm in a nitrogen glovebox. After annealing the thin film on a hot plate at 60 °C for 1 h and letting it rest at room temperature overnight, it was encapsulated in inert atmosphere between two quartz disks using epoxy resin (DELO-KATIOBOND LP655), as described in detail elsewhere.[63] The optical density of the solid sample was 0.26 at the visible maximum (~540 nm), which corresponds to a film thickness of about 45 nm, as inferred from the absorption coefficient published in the literature.[36] The steady-state absorption and fluorescence spectra of the encapsulated film revealed no sign of polymer degradation over a period of 1 month. For solution measurements, P3HT was dissolved overnight in chlorobenzene (Acros, Extra Dry, AcroSeal, 99.8%), which had previously been degassed by argon bubbling for 15 min. The solutions were placed in a 1 mm cell which consisted of two Spectrosil quartz disks separated by a Teflon spacer. The optical density at the visible maximum (455 nm) over 1 mm was 0.33 for the FU measurements with 500 nm excitation and 0.55 for 400 nm excitation, which corresponds to concentrations of about 0.08 mg/mL and 0.14 mg/mL, respectively. The shape of the absorption spectrum was the same at the two concentrations.

2.2. Steady-State Measurements. Steady-state absorption spectra were measured with a Cary 50 (Varian) spectrophotometer, while fluorescence emission and excitation spectra were recorded with a Cary Eclipse (Varian) fluorimeter (slit width 3 nm) and repeated with a Photon Technology International fluorimeter to verify reproducibility (slit width 2 nm, data not shown). All fluorescence spectra were corrected for the wavelength-dependent sensitivity of the detection. When representing the emission spectra on a wavenumber scale in cm^{-1}, the fluorescence intensity was multiplied by the square of the wavelength (λ^2) in order to account for the band-pass constant in wavelength imposed by the monochromator of the fluorimeter. All spectra shown here were recorded with the same solutions or thin film as used in the FU measurements. Similar spectral shapes were obtained with highly diluted solutions, so that concentration effects can be ruled out.

2.3. Time-Resolved Emission Measurements. Emission dynamics on the femtosecond time scale were obtained using the fluorescence up-conversion setup previously described.[63,64] In brief, the 800 or 1000 nm output of a tunable Mai Tai HP (Spectra-Physics) mode-locked Ti:sapphire laser system (100 fs pulse duration, 80 MHz repetition rate) was frequency doubled for sample excitation at 400 or 500 nm, respectively. The pump intensity per pulse was adjusted in the range of 6−40 $\mu J/cm^2$ (with a spot diameter of 20 μm) in order to keep the excitation density constant at the two excitation wavelengths. The latter was approximately 5×10^{13} or 4×10^{14} photons/cm^3 in solution (for two separate measurement sessions) and 1.5×10^{18} photons/cm^3 in the film. The measured sample fluorescence was detected by sum-frequency generation with a delayed gate pulse, and then the up-converted signal was dispersed in a monochromator and its intensity measured with a photomultiplier tube. The polarization of the pump beam was at the magic angle (54.7°) relative to that of the gate pulses, except for polarization-sensitive measurements, where it was set to 0° (parallel) and 90° (perpendicular). Measurements were done at room temperature in ambient conditions. To minimize degradation, the sample cell (containing the solution or thin film) was constantly rotated during the measurement. At least two scans of the dynamics in the −5 to 1000 ps (or 300 ps) range were averaged at each emission wavelength. No significant degradation of the samples was observed between two scans or when comparing the steady-state absorption and fluorescence spectra before and after the FU measurements.

2.4. Analysis of the FU Data. Again, details are described elsewhere,[63,65] so only a summary is given here. For each sample, the normalized time profiles obtained by FU at various emission wavelengths were analyzed globally using the convolution of a Gaussian-shaped instrument response function (IRF) with the sum of four exponential terms. The width of the IRF was found to be around 130 fs with the thin film and around 150−200 fs with solution samples. The wavelength-dependent amplitudes (or pre-exponential factors) were scaled to the steady-state emission spectrum, assuming that the steady-state emission intensity at a given wavelength is the time integral of the corresponding emission time profile. The time-resolved emission spectra were then reconstructed using the analytical expression for the time profiles at different wavelengths with the parameters (IRF, time constants, and scaled amplitudes) obtained from the fitting procedure. Note that the spectra obtained in this way are a convolution of the sample response and the IRF. This is why we only show spectra after 200 fs. A similar spectral shape would have been obtained if the spectra were directly reconstructed from the properly scaled raw experimental data; the reconstructed spectra are therefore not compromised by the number of fitting parameters, as long as they reproduce the data well. For femtosecond-resolved fluorescence anisotropy measurements, the anisotropy decay, $r(t)$, was calculated from the FU time profiles with the polarization of the pump beam parallel and perpendicular with respect to the gate beam, using the standard equation. This $r(t)$ was analyzed using the sum of exponential terms. The measured magic angle traces could always be well-reproduced by the data calculated from the parallel and perpendicular curves.

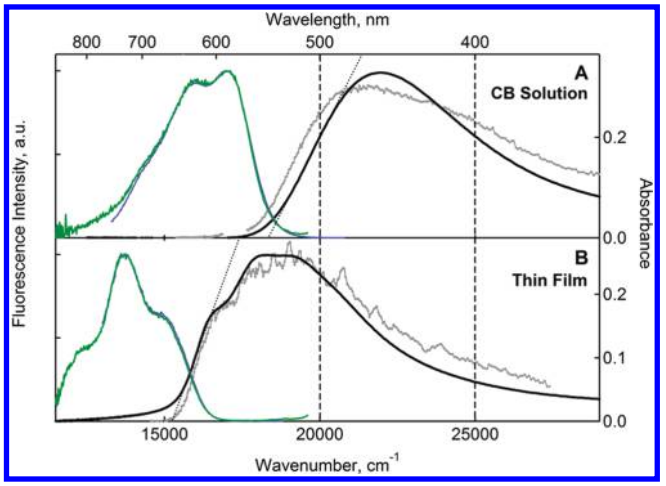

Figure 1. Steady-state spectra of P3HT in chlorobenzene solution (A) and as a thin film (B). The absorption spectra (thick black lines), the fluorescence excitation spectra probed near the emission maximum (gray lines with small markers), as well as the fluorescence emission spectra with 400 nm excitation (blue lines) and with 500 nm excitation (green lines) are shown. The excitation wavelengths (400 nm or 500 nm) used in the fluorescence up-conversion measurements are indicated as vertical dashed lines. The thin dotted lines identify the interband absorption edge from the absorption spectrum.

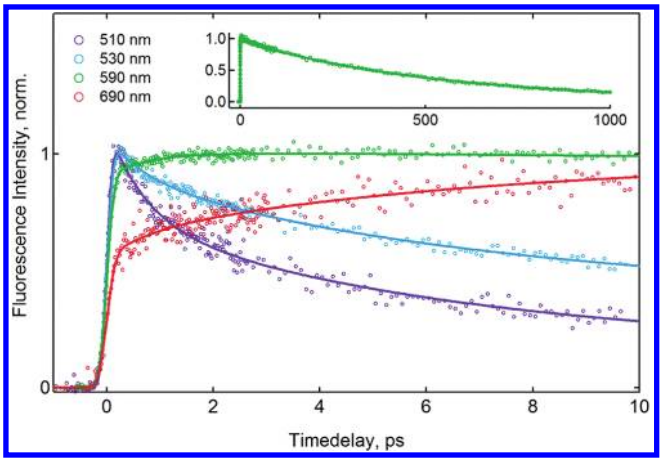

Figure 2. Ultrafast emission time profiles over 10 ps of P3HT in chlorobenzene solution after excitation at 500 nm. The probed emission wavelengths are shown in the legend. The solid lines correspond to the best multiexponential global fit. The inset shows the time profile of the 590 nm emission over 1000 ps.

3. RESULTS

3.1. Steady-State Spectra. As shown in Figure 1A, the visible absorption spectrum of P3HT dissolved in CB solution consists of a broad unstructured band with a maximum at 21 980 cm^{-1}, which we assign to the lowest energy $\pi-\pi^*$ interband transition. The band gap is estimated from the absorption edge as equal to 18 360 cm^{-1} (2.28 eV). The corresponding emission spectrum differs in shape from the absorption band, since it is much narrower and displays a vibronic progression. It peaks in the 0−0 band at 17 000 cm^{-1}, which implies a Stokes shift, i.e., energy difference between the emission maximum and the absorption edge, of 1360 cm^{-1} (0.17 eV). The emission spectra obtained with 400 and 500 nm excitation are so similar that they cannot be distinguished in Figure 1A, suggesting fast relaxation to a common emitting state, the singlet exciton. The fluorescence excitation spectrum we measured in solution is slightly broader than the absorption spectrum and displays structure (Figure 1A). This result could be reproduced at very low polymer concentration (absorbance ∼0.05) and using different fluorimeters. It is thus unlikely to be an artifact or a consequence of high sample absorption.

The absorption and emission spectra of P3HT thin film spin-cast from CB are considerably different from those of P3HT in solution, as shown in Figure 1B. The absorption spectrum is strongly red-shifted with a maximum at 18 280 cm^{-1}. It displays structure such as a pronounced shoulder at 16 780 cm^{-1}. The band gap is about 15 250 cm^{-1} (1.89 eV). The low-energy tail below the band gap is most probably due to midgap localized states, although there could be a contribution of increased reflection losses caused by changes in the refractive index near the band edge. The emission spectrum is also red-shifted in the film compared to solution; it is again independent of excitation wavelength, displays vibronic structure, and is much narrower than the absorption spectrum. The 0−0 transition is, however, less pronounced than in solution, whereas the 0−1 and 0−2 sidebands are enhanced. The 0−1 transition at 13 700 cm^{-1} is now clearly the emission maximum, giving a Stokes shift of 1550 cm^{-1} (0.19 eV). Within the experimental uncertainty, the fluorescence excitation spectrum in the P3HT film closely matches the absorption spectrum. It should be noted from the excitation spectrum that the absorption below the band gap (probably midgap states) does not significantly contribute to the emission.

3.2. Time-Resolved Emission for P3HT in Chlorobenzene Solution. *3.2.1. Excitation at 500 nm.* For P3HT in CB solution, excitation at 500 nm (2.48 eV) occurs on the low-energy side of the absorption spectrum (Figure 1A), with an excess energy relative to the band edge of 0.20 eV. The time profiles obtained by FU with 500 nm excitation at various emission wavelengths are depicted in Figure 2. The intensity decays almost to zero within the time window of 1 ns (see the inset), while the early emission dynamics are nonexponential and depend strongly on the emission wavelength. The fast decay at high energy and concomitant rise at lower energy suggest an initial red shift of the emission spectrum. This is in qualitative agreement with previous FU investigations of P3HT in chloroform solution (using lower molecular weight polymer and other excitation wavelengths).[16,37] Unlike those studies, many more emission wavelengths covering the entire spectrum were recorded here, and we chose to analyze the dynamics globally using the sum of four exponential functions. Time constants of τ_1 = 0.7 ps, τ_2 = 6.0 ps, τ_3 = 41 ps, and τ_4 = 530 ps were found, and the spectra of the pre-exponential amplitude factors are shown in Figure 3A. The amplitude spectrum of τ_4 is all-positive and identical to the steady-state emission spectrum. We therefore assign the 530 ps time constant to the decay of the relaxed singlet exciton, in excellent agreement with the lifetime reported in the literature.[36,37,54,55]

The three amplitude spectra related to the shorter time constants, $\tau_1-\tau_3$, are much weaker than the one of τ_4 and they are not related to any excited population decay (Figure 3A). They are positive (spectral decay) at low wavelengths and negative (spectral rise) at increasingly high wavelengths. This is characteristic of a progressive relaxation of the photoexcitation, leading to spectral changes. Our data and analysis provide us with

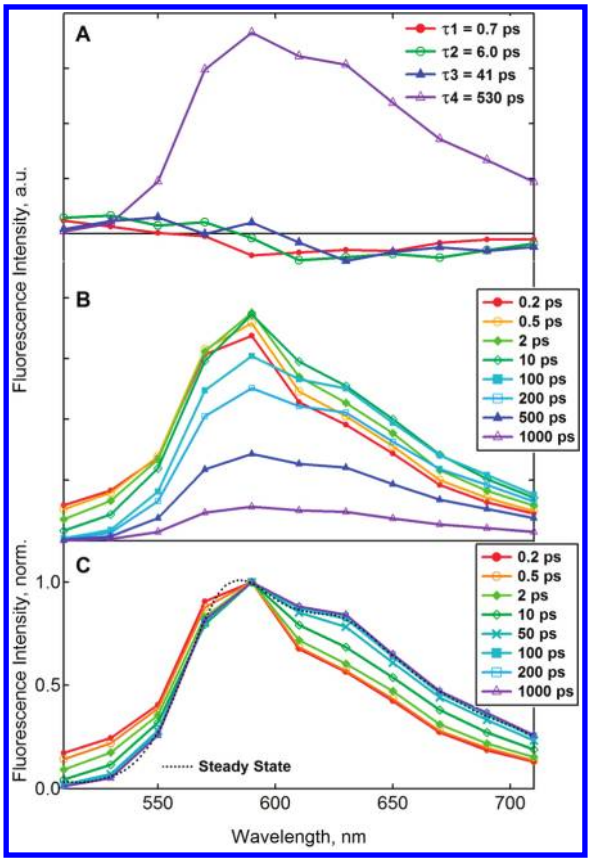

Figure 3. Outcome of the global analysis of the emission time profiles of P3HT in chlorobenzene solution after excitation at 500 nm: (A) decay associated amplitude spectra, (B) reconstructed time-resolved emission spectra, and (C) normalized reconstructed time-resolved emission spectra.

unique femtosecond-resolved emission spectra of P3HT, reconstructed from the global fitting parameters (Figure 3B). They are normalized in Figure 3C, for better visualization of the spectral shape evolution. The first emission spectrum that can be resolved with the FU instrumentation (at 0.2 ps) displays already >90% of the total Stokes shift, pointing to considerable relaxation on a ~100 fs time scale. It is also much narrower than the mirror image of the absorption spectrum and has relatively weak oscillator strength in the 0−1 vibronic band, compared to steady-state emission. After 200 fs, there is an important rise of the low-energy part of the emission spectrum over a few picoseconds (seen in the non-normalized spectra of Figure 3B). The spectrum also shifts to lower energy by about 0.013 eV (8% of the total Stokes shift) over tens of picoseconds (Figure 3C). Decay of the intensity below 550 nm occurs on the same time scale. The slowest relaxation in the emission spectrum, which only starts after about 1 ps, is the growth of the 0−1 vibronic sideband at 630 nm. This leads to an overall broadening of the spectrum and takes 100 ps to complete (Figure 3C).

3.2.2. Excitation at 400 nm. We also measured the emission dynamics of P3HT in CB solution following excitation at 400 nm. This occurs on the high-energy side of the absorption spectrum (Figure 1A), with 0.82 eV excess energy compared to the band edge. Figure 4A shows that the emission time profile at 580 nm is strongly affected by the excitation wavelength. There is a pronounced early rise only following 400 nm absorption.

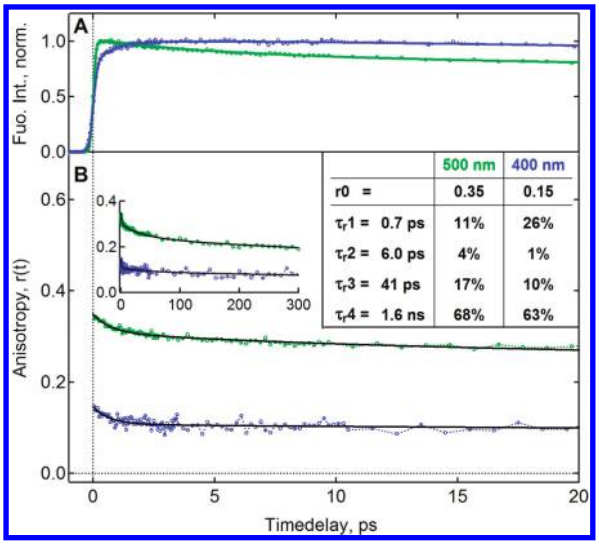

Figure 4. Ultrafast emission time profiles (A) and anisotropy decay (B) of P3HT in chlorobenzene solution recorded at an emission wavelength of 580 nm after excitation at 500 nm (green) and 400 nm (blue). The inset shows the anisotropy decay over a longer time scale. The solid lines correspond in each case to the best multiexponential fit. The fitting parameters obtained for the anisotropy decay are given in the inset table.

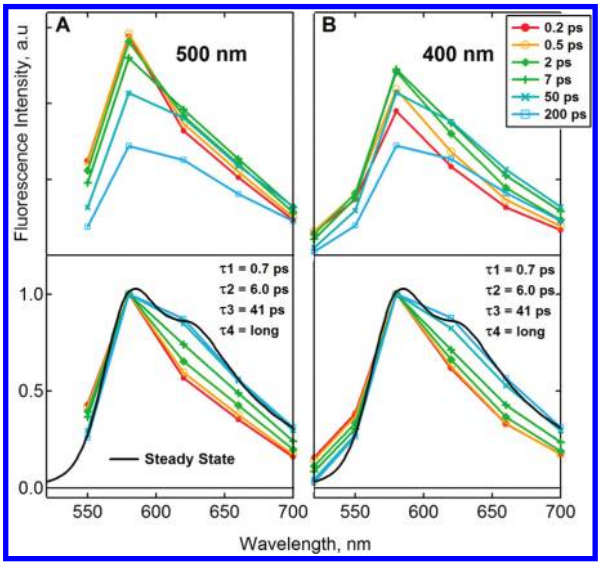

Figure 5. Outcome of the global analysis of the emission time profiles of P3HT in chlorobenzene solution after excitation at 500 nm (A) and 400 nm (B). The top panels show the reconstructed time-resolved emission spectra, while the normalized reconstructed time-resolved emission spectra are in the bottom panels.

The outcome of the global analysis of the time profiles recorded throughout the emission spectrum, following excitation at both wavelengths, is compared in Figure 5. The data were obtained under very similar conditions for 400 and 500 nm excitation, on a separate occasion and with a slightly higher excitation power than the data presented before for 500 nm (Figure 2,3), which explains the minor differences.

The early spectral rise, which occurs over a few picoseconds, is strongly affected by the excitation wavelength as shown on the top of Figure 5. It occurs only on the low-energy side of the

dx.doi.org/10.1021/jp1119348 |J. Phys. Chem. C 2011, 115, 9726–9739

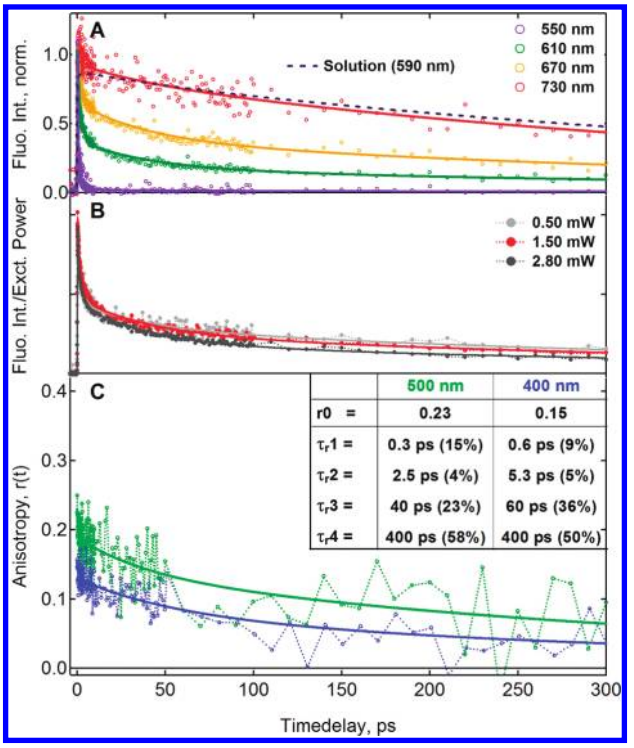

Figure 6. (A) Ultrafast emission time profiles of P3HT thin film after excitation at 500 nm. The probed emission wavelengths are shown in the legend. The dashed line shows the time profile of the 590 nm emission of P3HT in chlorobenzene solution after excitation at 500 nm. (B) Ultrafast emission time profiles of P3HT thin film recorded at an emission wavelength of 620 nm after excitation at 500 nm with different excitation intensities (the fluorescence intensity is divided by the excitation power). (C) Anisotropy decay of P3HT thin film recorded at 650 nm after excitation at 500 nm (green) and 400 nm (blue). The solid lines correspond in each case to the best multiexponential fit. The fitting parameters obtained for the anisotropy decay are given in the inset table.

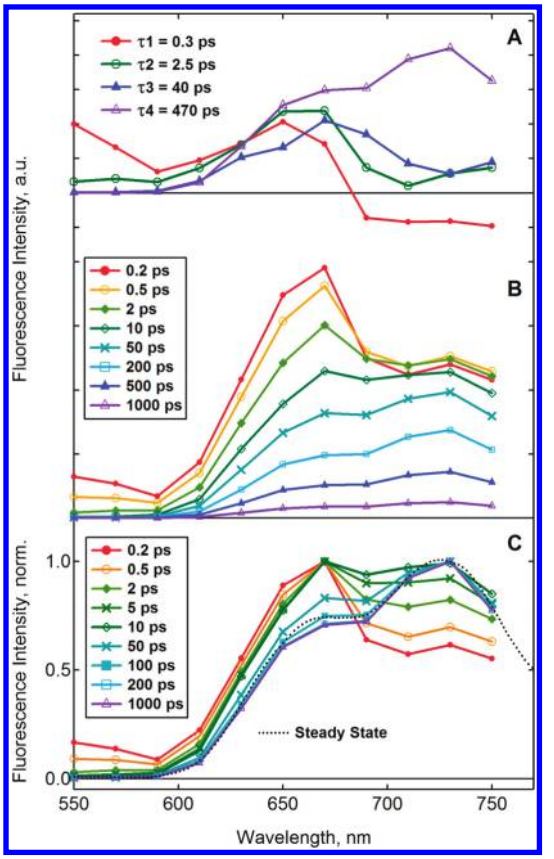

Figure 7. Outcome of the global analysis of the emission time profiles of P3HT thin film after excitation at 500 nm: (A) decay associated amplitude spectra, (B) reconstructed time-resolved emission spectra, and (C) normalized reconstructed time-resolved emission spectra.

emission spectrum with 500 nm excitation, while it is more pronounced and covers the entire spectrum with 400 nm excitation. The normalized emission spectra shown at the bottom of Figure 5 reveal, however, that the effective spectral shape and its time-resolved changes are much less dependent on excitation wavelength than the initial rise. The shape of the earliest resolved 0.2 ps spectrum, the spectral red shift, and the growth of the 0−1 vibronic sideband are all very similar with 400 and 500 nm excitation, and the time scales for the spectral relaxation are the same (0.7, 6.0, and 41 ps). This points to a weak dependence of the processes responsible for this spectral relaxation on the excitation wavelength. Note that τ_4, the exciton lifetime, could not be determined precisely for the data in Figure 5, as the dynamics were only recorded up to 300 ps. It can be said, however, that exciton decay occurs on a similar time scale (hundreds of picoseconds) at both excitation wavelengths.

3.2.3. Anisotropy Measurements. Finally, polarization-sensitive FU measurements were obtained and the calculated anisotropy at an emission wavelength of 580 nm is compared for 400 and 500 nm excitation in Figure 4B. The initial anisotropy r_0, measured with the 0.2 ps time resolution, is in both cases lower than the theoretical maximum of 0.4 (when the transition dipole moments of the absorption and emission are parallel). What is most interesting is that r_0 is considerably lower with 400 nm excitation (0.15) than with 500 nm excitation (0.35). After 0.2 ps, the anisotropy at 580 nm evolves in a quite similar manner for 400 and 500 nm excitation (Figure 4B). About 35% of r_0 is in both cases lost with time constants of 0.7, 6.0, and 41 ps, the same as for the spectral relaxation (see the inset table in Figure 4B). The remaining ∼65% of the initial anisotropy has a very long nanosecond lifetime, because the anisotropy in the isolated chains is now only lost by very slow orientational diffusion of the polymer molecule. We measured the anisotropy decay at several emission wavelengths throughout the spectrum, but found no significant difference within the experimental error (data not shown). This indicates that the emitting dipoles for the 0−0 and the 0−1 vibronic transitions are parallel.

3.3. Time-Resolved Emission for P3HT Thin Film. *3.3.1. Excitation at 500 nm.* For the P3HT spin-cast thin film, excitation at 500 nm occurs on the high-energy side of the absorption band with 0.59 eV excess energy compared to the band edge (Figure 1B). This is much more than the 0.20 eV excess energy injected in P3HT solution at the same excitation wavelength. The time profiles recorded in the film with 500 nm excitation also depend strongly on the emission wavelength, implying relaxation that leads to spectral changes (Figure 6A). We found time constants for the spectral relaxation in P3HT film of $\tau_1 = 0.3$ ps, $\tau_2 = 2.5$ ps, and $\tau_3 = 40$ ps, which are comparable but slightly faster than in solution. The outcome of the global analysis for the film data recorded with 500 nm excitation is shown in Figure 7. The amplitude spectra in panel A confirm that τ_1−τ_3 are due to

dx.doi.org/10.1021/jp1119348 |J. Phys. Chem. C 2011, 115, 9726–9739

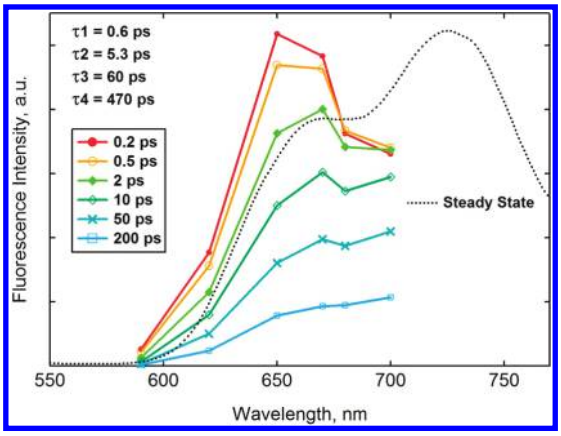

Figure 8. Reconstructed time-resolved emission spectra obtained by the global analysis of the emission time profiles of P3HT thin film after excitation at 400 nm.

spectral changes, while τ_4 = 470 ps is the exciton lifetime. The latter is on the same order of magnitude as the exciton decay observed in solution (530 ps). The similarity of the time scales is confirmed by the comparison of the fluorescence time profiles in the film (at 730 nm) and in solution (at 590 nm) shown in Figure 6A. Unlike in solution, the amplitudes of the significant spectral changes are comparable to the one of the exciton decay in the film.

Although we cannot obtain the entire emission spectrum due to experimental constraints above 750 nm, it appears that the shape of the earliest resolved spectrum at 0.2 ps (panels B and C of Figure 7) is already considerably narrower than the absorption spectrum. The overall spectral position is also close to the one for steady-state emission, showing that the majority of the Stokes shift has taken place faster than our time resolution. We note that the 0.2 ps spectrum in the film is very different from the corresponding spectrum in solution (strong red-shift), indicating a negligible contribution from nonaggregated (isolated) P3HT chains to the emission at this time delay. The earliest resolved spectrum in the film shows a well-resolved vibronic structure where both the 0−0 transition and the 0−1 sideband are visible, centered at 665 and 730 nm, respectively. A striking observation is the much higher relative intensity of the 0−0 band compared to the 0−1 band, the opposite of what occurs in the steady-state spectrum.

The normalized time-resolved emission spectra depicted in Figure 7C show that the relative intensity of the 0−0 band decreases in time. It has about the same intensity as the 0−1 band after 10 ps, and this inversion of the 0−0 and 0−1 relative intensity continues up to 200 ps, when the steady-state shape with a much more intense 0−1 band is reached. The amplitude spectra in Figure 7A show that the three first time constants, τ_1 = 0.3 ps, τ_2 = 2.5 ps, and τ_3 = 40 ps, are all associated with the decay of the 0−0 emission band. Apart from the inversion of the 0−0 and 0−1 relative band intensities, other spectral changes occur for P3HT film upon 500 nm excitation. The reconstructed time-resolved emission spectra in Figure 7B reveal a ∼1 ps spectral rise above 680 nm. The effect is quite weak compared to the solution measurements, but might be more pronounced on the red flank of the emission spectrum, which is experimentally not accessible. From the amplitude spectra in Figure 7A, it is clear that only τ_1 = 0.3 ps contributes to the initial spectral rise. Finally, Figure 7C shows enhanced early emission intensity below 600 nm, which decays with the τ_1 = 0.3 ps and τ_2 = 2.5 ps time constants. There is also a narrowing over 200 ps of the blue flank of the emission spectrum.

To ensure the absence of singlet exciton annihilation in our measurements, we varied the excitation intensity. The fluorescence time profiles scaled almost linearly with excitation intensity at the used pump power of 1.50 mW (see comparison with the dynamics obtained at a 0.50 mW excitation power in Figure 6B). Small effects of annihilation are seen at 2.80 mW. They became very important with a pump power of 8 mW, where τ_3 and τ_4 were reduced to 21 and 220 ps, respectively. The overall shape of the spectral changes was however not affected (data not shown).

3.3.2. Excitation at 400 nm. We also measured the FU time profiles of P3HT film following excitation in the high-energy tail of the absorption spectrum at 400 nm, with 1.12 eV excess energy compared to the band edge. The time-resolved emission spectra, reconstructed from the global analysis of the data, are depicted in Figure 8. There is hardly any difference compared to the data recorded with 500 nm excitation. Within the experimental uncertainty, the shape of the 0.2 ps spectrum is very close at the two excitation wavelengths. The spectral changes occurring after 0.2 ps, i.e., the narrowing on the blue side of the spectrum and the inversion of the 0−0 and 0−1 band intensities, are also very similar with 400 and 500 nm excitation. It is interesting to note that the initial spectral rise starts at 680 nm independently of the excitation wavelength, in contrast to the higher-energy start of the rise observed with 400 nm excitation compared to 500 nm excitation in solution (Figure 5A). The strong decay of the 0−0 band in the P3HT film probably masks any spectral rise in the high-energy part of the spectrum. The only evidence that more relaxation is needed in the film when more excess energy is initially provided is that the time constants for the spectral relaxation are slower with 400 nm excitation (τ_1 = 0.6, ps, τ_2 = 5.3 ps, and τ_3 = 60 ps).

3.3.3. Anisotropy Measurements. Finally, the anisotropy decay of the 620 nm emission, with both excitation wavelengths, is shown in Figure 6C. The initial anisotropy measured within the 200 fs time resolution is much lower than 0.4. Again, r_0 is smaller with 400 nm excitation (0.15) than with 500 nm excitation (0.23). The difference is less pronounced than in solution, where r_0 with 500 nm excitation was higher (Figure 4B). At both excitation wavelengths, about 50% of the initial anisotropy decays with the same time constants as the spectral relaxation (inset table in Figure 6C). The remaining anisotropy decays with a 400 ps time constant, clearly faster than the nanosecond anisotropy decay component in solution (Figure 4B), but slower than the spectral relaxation.

4. DISCUSSION

On the basis of experimental results obtained from photoconductivity studies and ultrafast investigations of the infrared active vibrational (IRAV) modes in PPV and MEH-PPV[66−71] and on evidence obtained from highly oriented MEH-PPV chains in a polyethylene matrix,[72−75] we view conjugated polymers as quasi-one-dimensional semiconductors and describe their electronic structure within an energy band picture.[1,62] We note here that the band versus molecular interpretation is not directly relevant to the scope of the current paper. The important point is that absorption leads to a delocalized primary photoexcitation, which then relaxes to a more localized exciton state. As

discussed in the following, the initial delocalization has been shown by several independent groups and was not necessarily described within the semiconductor approach. Several processes contribute to the relaxation of the primary photoexcitation of P3HT to the relaxed singlet exciton: (1) self-localization, (2) exciton formation, (3) exciton hopping, and (4) slow torsional rearrangements. They will be discussed on the basis of our time-resolved emission results.

4.1. Interpretation of the Steady-State Spectra. We interpret the visible absorption spectrum of P3HT as an allowed $\pi-\pi^*$ interband transition yielding electrons and holes in the conduction and valence band, respectively. Emission on the other hand occurs from a relaxed singlet exciton state. In our solution measurements, both absorption and emission are essentially intrachain processes within isolated polymer chains. Indeed, polymer aggregation (between chains and due to chain folding) is considered negligible at the concentrations used and given the fact that CB is a "good" solvent. Our absorption and emission spectra are also consistent with the spectral shapes reported previously for nonaggregated P3HT in dilute solution.[40] Strong conformational (mostly torsional) disorder of the dissolved P3HT chains in the ground state leads to the inhomogeneously broadened and structureless absorption spectrum. The difference between the absorption spectrum and the broader/more structured fluorescence excitation spectrum indicates that the fluorescence quantum yield differs within the distribution of absorbing conformations. The more fluorescent conformers are on both sides of the absorption band, while the less fluorescent ones absorb in its center.

The shape of the emission spectrum in solution is independent of excitation wavelength. Even if a large distribution of conformations is initially excited, relaxation eventually occurs to a common emitting intrachain exciton state with less torsional disorder. Judging from the excitation spectrum, the low-fluorescent conformations relax to this state in lower yield. The relaxation toward a more localized singlet exciton after the initial interband absorption and toward higher order explains the narrower and more structured emission spectrum. The intrachain emission spectrum has previously been well-reproduced with a Franck−Condon model, using a Huang−Rhys factor of 1 and assuming that the 0.18 eV C=C stretching vibration predominantly couples to the electronic transition.[40] A structured emission spectrum contrasting with a broad absorption spectrum was also observed for phenyleneethynylene oligomers in solution, where the effect was as well ascribed to a more planar and conformationally constrained excited state compared to a torsionally disordered ground state.[76]

The considerable differences between the solution and thin film steady-state spectra can be accounted for by the self-organization of P3HT into microcrystalline π-stacked lamellar sheets in the film. This brings interchain character to the absorption and emission transitions. Although several models have been proposed for the film spectra,[44,45] the most successful one is given by Spano.[42,43,77] Here, the P3HT chains in the film are treated as weak H-aggregates. The excitonic coupling between chains is lower than the exciton−phonon coupling, as the excitonic interactions are decreased due to the important conjugation length within the polymer chains. The low-energy side of the $\pi-\pi^*$ absorption band of thin film P3HT can be well-modeled using H-aggregates as the absorbing species.[29,40,42,43] All the vibrational structure occurs in this part of the spectrum, and the relative absorbance of the 0−0 and 0−1 vibronic peaks gives access to the excitonic coupling energy, which is related to the conjugation length. The presence of vibronic structure (not completely masked by inhomogeneous broadening) indicates less ground state conformational disorder in the H-aggregates compared to the P3HT chains in solution, i.e., there is a smaller distribution of torsional conformers and conjugation lengths in the more extended and planar polymer chains of the film.

The high-energy side of the broad absorption band of P3HT film cannot be reproduced with the H-aggregate model. Clark et al. suggested that this part of the spectrum has a strong contribution from nonaggregated (amorphous, disordered) P3HT chains, with intrachain absorption and about 40% less oscillator strength than the H-aggregates.[29,40] They noticed that the shape of the high-energy film absorption strongly resembles the structureless solution spectrum, once the H-aggregate part of the spectrum is subtracted. After photoexcitation of the disordered P3HT chains, there is, however, relaxation toward H-aggregates. The shape of the steady-state emission spectrum is independent of the excitation wavelength and thus always arises from the same species. The similarity of the fluorescence excitation and absorption spectrum also confirms that the relaxation to a common emitting state (the interchain singlet exciton) is near quantitative, independently of where P3HT is initially excited. Note that, unlike in solution, there is little effect of torsional disorder on the excitation spectrum in the film. The emission spectrum of P3HT film has been previously modeled using H-aggregates as the sole emitting species; it can be reproduced using a modified Franck−Condon expression with a Huang−Rhys factor of 1 and a vibrational progression dominated by the 0.18 eV C=C stretching vibration.[40] The 0−0 transition is forbidden in the H-aggregates (although it can be enhanced by disorder and thermal activation) while the sidebands are allowed. Hence the 0−1 transition is the band maximum in the emission spectrum of P3HT film.

4.2. Ultrafast (<200 fs) Relaxation Processes. The time-resolution of our FU instrumentation does not allow us to directly measure processes occurring on the ~100 fs time scale. A lot can nevertheless be learned about this ultrafast relaxation by looking at its consequences on the shape of the earliest resolved 0.2 ps emission spectrum and the initial anisotropy. For P3HT in both solution and film, >90% of the total Stokes shift takes place faster than 0.2 ps, and there is important loss of anisotropy which is higher with 400 nm excitation than 500 nm excitation. The 0.2 ps spectrum is also narrower than the mirror image of the absorption spectrum, and its shape does not significantly depend on excitation wavelength. All these observations point to considerable relaxation during the 200 fs that follow $\pi-\pi^*$ interband absorption in P3HT, which we ascribe to self-localization of the initially delocalized photoexcitation.

Light absorption in conjugated polymers yields mobile electrons and holes within the energy bands, which are considerably delocalized along the polymer chain. Self-localization of the charge carriers into a smaller number of repeat units within 100 fs, associated with local structural lattice distortions that are strongly coupled to the electronic excitation, has been predicted 30 years ago.[78] The self-localization of the primary photoexcitation has recently been experimentally observed for many polymers, including polythiophene derivatives.[19,30,34,79−84] Dynamic localization in MEH-PPV was, for example, observed by a faster decay of the polarization anisotropy in the fluorescence and TA dynamics, as compared to derivatives with shorter conjugation length,[79] as well as by three-pulse photon echo experiments in

films and solution.[80,81] In the latter study, absorption into delocalized states that arise from electronically coupled polymer segments was suggested to model the data. The localization of the primary photoexcitation, which was found to be delocalized over at least 11 nm in MEH-PPV,[79] is largely driven by local geometrical relaxation from the more twisted geometry of the ground state to a planar quinoidal structure in the excited site.[19,30,34,37,79−81] This process in P3HT is dominated by only two phonon modes: the 0.18 eV C═C stretching vibration and a lower frequency (∼0.016 eV) torsional motion.[30] There is evidence that it is not a stochastic but a correlated process.[30] The correlation of transition frequencies within the ensemble of excitations was also observed by Collini and Scholes for MEH-PPV chains in solution.[85] Those authors conclude that the high delocalization of the primary excitation allows its quantum mechanical transport in space by coherent excitation energy transfer on the ∼100 fs time scale. Ultrafast migration of the primary photoexcitation is therefore possible, although this occurs by a very different mechanism than the much slower incoherent hopping of a bound exciton (Förster mechanism, discussed in section 4.3).[83]

4.2.1. Self-Localization in Isolated P3HT Chains. As mentioned before, the important Stokes shift (>90%) occurring for the emission of P3HT in CB solution within 200 fs is evidence of the initial photoexcitation localization. Moreover, we found that the 0.2 ps emission spectrum has already considerably narrowed compared to the absorption spectrum, which is a consequence of the localization and of the ultrafast geometrical relaxation driving this localization. Ultrafast torsional relaxation obviously reduces inhomogeneous broadening, implying that the conformational disorder in the ensemble of emitting species has been reduced compared to the ground state distribution. Selective excitation of certain torsional conformers with 500 nm excitation is unlikely as the origin of such a pronounced narrowing of the emission spectrum, since the laser pulse is relatively broad and carries excess energy, so that a distribution of conformers is excited. The very similar shape of the 0.2 ps spectrum obtained following 400 and 500 nm excitation is unexpected, since different torsional conformers within the inhomogeneous distribution are excited. Apparently, any differences in the excited conformers are evened out during the ultrafast ∼100 fs local structural rearrangements.

The very strong emission depolarization during the initial <100 fs self-localization is caused by several processes: The local structural (torsional) rearrangements, the localization of the initially delocalized excitation around kinks and bends in the polymer chain (which reorients the dipole), and the quantum-assisted transport of the delocalized excitation.[37,79,83−85] We observe a considerably lower initial anisotropy with 400 nm excitation (0.15) than with 500 nm excitation (0.35), clearly in contrast with our previous result in PCDTBT, where r_0 was about 0.3 at both wavelengths.[63] The wavelength-dependence of r_0 is, however, consistent with a transient absorption study by Guo et al., where the initial anisotropy in the excited-state absorption of regiorandom P3HT film was found to by much higher upon 500 nm compared to 400 nm excitation.[26] Our results evidence more relaxation and more initial delocalization of the primary photoexcitation in isolated P3HT chains if absorption at higher energy occurs higher into the energy bands. With more initial delocalization, the self-localization leads to more loss of the initial polarization memory and gives a lower measured r_0. Our data agrees with a previously reported intermediate value of r_0 (∼0.25) for P3HT in chloroform following excitation at 470 nm.[37] The authors also observed that r_0 decreases with increasing polymer molecular weight, which might also be an effect of increased delocalization.

4.2.2. Self-Localization in P3HT Film. As in solution, ultrafast <200 fs localization of the primary excitation in P3HT film manifests as an important Stokes shift, emission depolarization, and narrowing of the 0.2 ps spectrum. Due to the interchain interactions of the P3HT aggregates formed in the film, the initial delocalization spans neighboring polymer chains. This favors the formation of long-lived delocalized polarons by the self-localization of the electrons and holes on separate polymer chains.[46,49−51] The yield of macroscopic charge carriers in P3HT film is as high as 30%,[38] but since they are formed during the <100 fs self-localization,[26] they have no effect on the emission dynamics resolved in our experiments. Again, r_0 is lower with 400 nm excitation (0.15) than with 500 nm excitation (0.23) in the film, because of the increased initial delocalization and increased relaxation if excitation occurs higher into the energy bands. The difference is less pronounced than in solution, because more excess energy is brought to the film than to P3HT solution at 500 nm, and because the interchain character of the absorption allows a higher initial delocalization in the film at any excitation wavelength.

We note that the 0.2 ps emission spectra recorded in the film following 400 or 500 nm excitation are quite similar and relatively close in energy to the steady-state emission, which stems solely from H-aggregates. This is somewhat surprising, since it has previously been determined that about 55% of the P3HT chains in films cast from high boiling point solvents are amorphous and have an absorption spectrum similar to dissolved P3HT.[29] A high proportion of amorphous P3HT is excited at 500 nm, while amorphous chains are almost exclusively excited at 400 nm. Similar to absorption, the emission spectrum of amorphous P3HT should be close to that of the isolated polymer in solution, i.e., have a 0−0 emission maximum around 585 nm and high fluorescence quantum yield (isolated P3HT in solution has a quantum yield of 33%, versus 2% in thin film[36]). The emission maximum for P3HT film at 0.2 ps is, however, at 665 nm independent of the excitation wavelength, and the intensity in the 585 nm region is only very slightly enhanced compared to the steady-state spectrum. This suggests that relaxation to aggregates occurs in <200 fs, so that there is no significant contribution of amorphous P3HT emission already after 0.2 ps.

There are two possible explanations for this phenomenon. First, the polymer chains absorbing at high energy might not be completely isolated/amorphous but rather in poorly crystalline aggregates, where the P3HT chains are still parallel but interact less due to high disorder. In solution, we observed a decrease of torsional inhomogeneity during the <200 fs geometrical relaxation. This is likely to occur also in the film and might be enough to convert the more disordered aggregates to more ordered and crystalline species on an ultrafast time scale. The second possibility is that the photoexcitation migrates from amorphous to crystalline polymer regions within <200 fs. This raises the same question that we recently brought up concerning the transport of the photoexcitation to an interface in polymer:fullerene bulk heterojunction blends, prior to charge separation:[63] How can the excited species move so fast? An exciton diffusion coefficient of 1.8×10^{-3} cm^2 s^{-1} was reported for P3HT,[86] which means that an exciton can diffuse on the 100 fs time scale by about 0.1 nm (in one dimension) or 0.2 nm (in three dimensions). The separation between amorphous and crystalline polymer regions should be much longer, on the order of 10 nm, so that exciton hopping by

the Förster mechanism (see section 4.3) is too slow to account for the ultrafast migration between those regions. We therefore suggest that it is not the bound exciton that diffuses on the ~100 fs time scale but its delocalized precursor. Indeed, the electron and hole formed directly after interband absorption are expected to be mobile and delocalized, making ultrafast transport of the primary photoexcitation by quantum mechanical mechanisms possible.[85]

4.3. Exciton Formation and Hopping. After 0.2 ps, the emission spectrum of P3HT in solution and as a thin film continues to evolve to lower energy. This relaxation can be resolved by our experiments, and we found in each case three associated time constants ranging from subpicoseconds to tens of picoseconds. As the different relaxation processes responsible for the spectral changes are complex and occur in parallel, it is impossible to assign each time constant to a specific relaxation route. Nevertheless, the time constants found from the global analysis provide a good estimation of the time scales over which the relaxations occur.

We suggest that the emission at 0.2 ps does not yet originate from a relaxed singlet exciton. When the time-resolved emission spectra are considered without normalization, a fast rise of the emission spectrum is observed (more obvious for the solution measurements). In agreement with our recent fluorescence study of the donor−acceptor copolymer PCDTBT,[63] we ascribe this early spectral rise and the fastest time constant (of the order of 0.5 ps), at least partially, to slower components of singlet exciton formation. This involves thermalization of the electron and hole to the band edges, as well as their spatial recombination and Coulomb binding. In solution, the early spectral rise occurs only on the low-energy side of the emission spectrum with 500 nm excitation, while it is more pronounced and covers the entire spectrum with 400 nm excitation. This shows that the electrons and holes have to relax further through the energy bands to the band edges in order to form the exciton, if they are initially excited higher into the bands. It confirms our assignment of the spectral rise to exciton formation and provides evidence that this process is relatively slow (~1 ps). In the film, the exciton formation also occurs on the ~1 ps time scale, but we could not find the spectral dependence of the rise on the excitation wavelength, probably because it is masked by other spectral changes. Note that the excitons in the P3HT film are interchain species with some delocalization between π-stacked polymer chains.

After they have formed, the singlet excitons can hop to lower-energy localized states, allowing a change of their spatial position and energy.[37] The process has often been described as excitation energy transfer, mainly by the Förster mechanism, between polymer segments of different conjugation lengths that exist due to disorder (kinks and defects in the polymer chain).[37,57,63,83,84,87−97] Cascading down-energy exciton migration typically leads to a progressive red shift of the emission spectrum, which slows down in time as the number of nearby states with lower energy decreases. Multiphasic time scales ranging from about half a picosecond (for one-step hops) to hundreds of picoseconds (for multistep hops) were reported for various polymers, so that we conclude that exciton hopping contributes to the three time constants we found for the spectral relaxation of P3HT in solution and film.

In solution, exciton migration leads to a red shift of the emission spectrum by about 0.013 eV (8% of the total Stokes shift) over tens of picoseconds and a considerable decay of the emission intensity below 550 nm on the same time scale. Exciton hopping to states with a different orientation of the transition dipole moment also contributes to the emission depolarization that occurs with the same time constants as the spectral changes. Note that excitons do not only move to lower energy sites but also to sites with similar energy. The isoenergetic hops can lead to depolarization, but not to any shift of the emission spectrum. In principle, higher energy excitation should lead to the initial formation of higher energy excitons, which have more probability to hop to lower energy localized states, so that exciton hopping in P3HT could be affected by the excitation wavelength, as was reported for the PPV polymer.[90] Judging from the normalized emission spectra, the spectral changes and time constants associated with exciton hopping are, however, quite independent of 400 or 500 nm excitation in solution. The wavelength-dependent spectral rise that we observe 1−2 ps after photoexcitation might have a contribution from the population of more red-shifted states by hopping. The rise is nevertheless too fast to be accounted for entirely by (multistep) Förster energy transfer processes. Our assignment to exciton formation is thus justified.

In the film, exciton hopping can be intrachain or interchain and contributes to a narrowing on the blue flank of the emission spectrum over 200 ps. We also observe somewhat enhanced early emission intensity below 600 nm, which decays with the two faster time constants (τ_1 = 0.3 ps and τ_2 = 2.5 ps, following 500 nm excitation). This is mostly related to remaining high-energy excitations on disordered polymer segments with short conjugation lengths, which decay rapidly due to exciton hopping to lower-energy, more-ordered sites. This effect is nevertheless weak, as most relaxation toward more ordered species takes place during the initial self-localization. The spectral changes occurring after 0.2 ps due to exciton hopping are very similar with 400 and 500 nm excitation in the film, but the time constants associated with the relaxation are slightly slower with higher energy excitation. At both excitation wavelengths, about 50% of the initial anisotropy decays with the same time constants as the spectral relaxation, partly due to exciton hopping. The remaining anisotropy decays with a 400 ps time constant, clearly faster than the nanosecond anisotropy decay component in solution, but slower than the spectral relaxation. The 400 ps depolarization in the film is ascribed to isoenergetic exciton hops between neighboring polymer chains. Due to the high ordering of the P3HT chains, this anisotropy decay is much slower than the 50−60 ps depolarization caused by interchain hops in amorphous PCDTBT film.[63]

4.4. Evolution of the Vibronic Structure in P3HT Emission. *4.4.1. The Vibronic Structure in Solution.* The time-resolved emission spectrum of P3HT measured in solution after 0.2 ps is dominated by the 0−0 transition. In spite of the strong electron−phonon coupling in conjugated polymers, the shoulder due to the 0−1 vibronic band is much less pronounced at early time delays than in the steady-state emission spectrum, indicating that the 0−1 transition of the emitting species a few hundred femtoseconds after photoexcitation is somewhat forbidden. The 0−1 vibronic sideband at 630 nm then grows over 100 ps, leading to broadening of the emission spectrum. This relaxation only starts after about 1 ps, after the excitons have formed and have perhaps even undergone one-step hops. We ascribe the growth of the 0−1 band to slow torsional relaxation of the P3HT chains toward a more planar structure. In general, conjugated systems tend to adopt a more planar configuration in the singlet exciton state than in the ground state.[98,99] As discussed before,

some of the more local geometrical relaxation occurs on the ultrafast time scale and is responsible for self-localization of the photoexcitation. The slower torsional rearrangements are associated with low-frequency vibrations and involve a conformational change over a larger portion of the polymer backbone (several repeat units). It has also been suggested that they are thermally activated.[37]

Slow excited-state planarization of a polythiophene derivative in toluene solution has been reported to occur in 15 ps and to lead to an increase of conjugation length by about two repeat units.[88] For P3HT in solution, the torsional relaxation responsible for the change in vibronic structure contributes to the 6 and 41 ps time constants of the spectral relaxation and possibly also causes some spectral red shift. Within the experimental uncertainty, the process is independent of the excitation wavelength. As the rearrangements can reorient the emitting dipole, they contribute, together with exciton hopping, to the emission depolarization on the picosecond/tens of picoseconds time scale. Due to its similar time scale and effect on the conjugation length, torsional relaxation is strongly entangled with exciton hopping. It has been suggested that torsional relaxation becomes the predominant mechanism for shorter polymer chains or with low excitation energy, when exciton hopping becomes less favored.[37,88]

Spectral relaxation due to torsional relaxation has been investigated in detail for conjugated oligomeric model systems in solution.[76,100,101] In those studies, the planarization typically leads to a red shift of the spontaneous or stimulated emission spectrum, together with a decrease of the inhomogeneous broadening of the vibronic bands, so that the spectrum becomes more structured. This clearly differs from the spectral broadening brought about by the growth of the 0−1 sideband seen here for P3HT in solution. A decrease of the inhomogeneous broadening is not at the origin of the slow appearance of this vibronic sideband, since the spectrum has already considerably narrowed during the <200 fs relaxation processes. This leads to the conclusion that the slow torsional relaxation in P3HT really enhances the oscillator strength of the vibronic 0−1 transition, possibly by increasing the Franck−Condon coupling between the electronic excitation and the predominantly Franck−Condon active C═C stretching vibration. Further theoretical work is necessary to understand why the 0−1 emission is so small in the species formed after the <200 fs ultrafast geometrical changes causing self-localization and how the slower structural changes then enhance this transition.

4.4.2. The Vibronic Structure in the Thin Film. In the emission spectrum of P3HT film 0.2 ps after light absorption, the relative intensity of the 0−0 band is strikingly higher compared to the 0−1 band. As discussed before (section 4.2.2), we are confident that the early emission stems already from P3HT aggregates, even if amorphous or disordered P3HT regions are initially excited. The important 0−0 intensity indicates, however, that they are not yet relaxed H-aggregates, for which the 0−0 transition is symmetry forbidden.[43,102] We observe a decrease of the 0−0 emission intensity occurring with the three time constants of the spectral relaxation (0.3, 2.5, and 40 ps with 500 nm excitation), until the steady-state spectrum with a 0−1 band maximum is reached. The significant decay of the 0−0 band with the 0.3 ps time constant (which is largely associated with thermalization to the band edges and exciton formation) is consistent with the theoretical result of Spano et al. that the 0−0 oscillator strength is higher when the electron and hole are toward the top of the energy bands.[77] The 0−0 emission therefore decreases rapidly during thermalization to the band edges. It continues to decrease more slowly, which we mainly assign to torsional relaxation leading to a planarization of the entire polymer backbone, as described earlier in the context of the solution data. The torsional relaxation also contributes, together with exciton hopping, to the narrowing observed over 200 ps on the blue flank of the emission spectrum and to emission depolarization. It is very similar with 400 and 500 nm excitation.

The steady-state emission spectrum of P3HT in solution (isolated chains) and in the film (H-aggregates) has been modeled with a Franck−Condon expression and a Huang−Rhys factor of 1 (for the film data, the 0−0 amplitude is variable and uncoupled from the rest of the progression).[40] The same model was used to describe the emission spectra of P3HT diluted in an inert ultrahigh molecular weight (UHMW) polyethylene matrix at different concentrations; again a Huang−Rhys factor of 1 independent of the extent of aggregation was found.[17] We did not perform a quantitative Franck−Condon analysis of our time-resolved emission spectra, given the rather limited number of spectral points. Qualitatively, it appears, however, that the Huang−Rhys factor changes with time, leading to the decrease of the 0−0 band intensity. The Huang−Rhys factor represents the coupling of the electronic excitation to the Franck−Condon active vibrational modes (in this case predominantly the 0.18 eV C═C stretching vibration), which depends on the displacement of the nuclear potential wells in the ground and excited states. We suggest that slow torsional relaxation, involving low-frequency modes that are not necessarily Franck−Condon active, shifts the equilibrium position of the C═C vibration in the excited state. As a consequence, the potential well as a function of the C═C stretching coordinate shifts and hence the Hung−Rhys factor changes.

Torsional relaxation to a more planar polymer chain configuration also increases order in the polymer chain, which affects the vibronic structure of the emission spectrum. Indeed, remaining disorder after the initial self-localization, but before the slower planarization, can lift the symmetry constraints and explain the presence of the symmetry-forbidden 0−0 band. Simulations of the steady-state spectra have shown that disorder enhances the 0−0 emission, while it hardly affects the vibronic sidebands.[77] It is interesting to mention here that the 0−0 transition is also thermally activated, i.e., more pronounced at room temperature compared to 10 K.[77,102] It has recently been observed for P3HT in an UHMW polyethylene matrix that the emission time profiles recorded in the 0−0 band and 0−1 band only depend on the emission wavelength for high P3HT concentration, proving the important role of aggregates in the spectral changes.[17] Vibrational cooling mediated by torsional relaxation was used to explain the result. In this case, the enhanced early emission in the 665 nm region (near the 0−0 band) originates from vibrationally hot excited aggregate states with more torsional disorder and symmetry-allowed transitions to the electronic ground state (same parity).[102] After vibrational relaxation to the lowest vibrational level in the electronically excited state, the 0−0 transition at 665 nm becomes forbidden.

The inversion of the vibronic bands that we report for pristine P3HT film is unlikely to be a relaxation from nonaggregated to aggregated sites by exciton hopping, as was suggested on the basis of a similar observation for P3HT film at 10 K recorded on the nanosecond time scale.[40] This would imply a stronger

spectral red-shift, which we do not observe at room temperature (the position of the 0−0 band shifts by only about 0.015 eV, while the 0−1 band does not shift at all between 0.2 and 200 ps). Exciton migration to interchain aggregates has been observed for films of PTOPT, a substituted polythiophene derivative with close interchain packing but less crystallinity than P3HT, and there was indeed a much more pronounced red shift.[48] Kobayashi et al. explained the inversion of the 0−0 and 0−1 emission intensities observed for a regioregular polythiophene derivative at low temperature (measured with a streak camera and 7 ps resolution) by emission from two distinct intrachain states of opposite parity and with different lifetimes.[44] As it has today been well-established that absorption and emission in P3HT films has interchain character, this interpretation is less likely.

4.5. Exciton Decay. In solution, we found a 530 ps time constant for the decay of the relaxed singlet exciton, in excellent agreement with the lifetime reported in the literature.[36,37,54,55] A major deactivation channel of the intrachain exciton in isolated P3HT chains is intersystem crossing to the triplet state; emission occurs with a quantum yield of about 30% in CB.[36,55] Singlet annihilation as a decay mechanism can be excluded here, since the time constants showed no dependence on the excitation power at the low intensities used. In the film, we measured an exciton lifetime of 470 ps, again in accordance with previously published values.[17,36] This is on the same order of magnitude as the exciton decay observed in solution. The strong reduction of the fluorescence quantum yield from 33% to 2%,[36] when going from solution to film, can therefore not be explained by a reduction of the exciton lifetime. It is rather due to the high yield of nonemitting polarons in the P3HT films directly from the primary photoexcitation[36,38] and due to the lower oscillator strength for emission in H-aggregates compared to free polymer chains.[40,46] Intersystem crossing of singlet intrachain excitons to the triplet state was observed in transient absorption studies of P3HT solution and in regiorandom P3HT films, but the interchain character of the singlet excitons in regioregular P3HT films was found to prevent formation of triplet excitons.[26,36,46] We therefore assign the 470 ps interchain exciton decay in the P3HT film to nonradiative exciton recombination to the ground state. Although the ∼500 ps exciton decay of H-aggregates in the film and of free polymer chains in solution is in both cases predominantly nonradiative,[17] we conclude that it occurs by different mechanisms.

5. CONCLUSIONS

Detailed fluorescence up-conversion measurements, followed by global analysis of the emission time profiles and reconstruction of the time-resolved emission spectra with a 200 fs resolution, allowed a comprehensive understanding of the photophysics of pristine regioregular P3HT in dilute chlorobenzene solution and solid thin film. The isolated P3HT chains in solution are torsionally highly disordered in the ground state, leading to an inhomogeneously broadened, structureless absorption spectrum. The absorption is assigned to an interband $\pi-\pi^*$ transition that is entirely intrachain. On the other hand, the $\pi-\pi^*$ absorption in spin-cast P3HT film has interchain character, since the polymer organizes into microcrystalline π-stacked lamellar sheets. This yields a strongly red-shifted spectrum where a vibronic structure can by discerned, as the ordering reduces the inhomogeneous broadening. There is nevertheless remaining torsional disorder in the film, explaining why only the low-energy part of the spectrum can be modeled as absorption by H-aggregates. The high-energy absorption arises from amorphous polymer chains or highly disordered P3HT aggregates.

In both film and solution, the initially highly delocalized and mobile electrons and holes, formed in the energy bands by the $\pi-\pi^*$ interband absorption, self-localize within ∼100 fs. This relaxation is driven by ultrafast local geometrical relaxation involving the C=C stretching and a torsional vibrational mode. The ultrafast localization explains why the earliest emission spectra that we could measure 0.2 ps after excitation are already strongly Stokes-shifted (>90%). In film and solution, the shape of the earliest 0.2 ps emission spectrum displays much less inhomogeneous broadening than the absorption spectrum, showing that the <200 fs processes effectively decrease the torsional disorder. The early 0.2 ps emission spectrum is also virtually independent of the excitation wavelength, indicating that any differences due to selective excitation of certain conformers in solution or amorphous/crystalline regions in the film are evened out on the ultrafast time scale. We made the important observation that emission in the film only 0.2 ps after photoexcitation occurs mainly from aggregates, even if a high proportion of amorphous/disordered P3HT chains is initially excited. Either the ultrafast geometrical relaxation is sufficient to convert the disordered polymer to more crystallinity or the photoexcitation can migrate from amorphous to ordered regions in <200 fs. This migration is too fast to be accounted for by Förster hopping of a bound exciton, so we suggest instead quantum mechanical transport of the primary delocalized photoexcitation.

Moreover, for the dilute and solid sample, we observed a strong loss of the emission anisotropy during the ultrafast relaxation, caused by the local structural rearrangements, by the localization of the initially delocalized excitation around kinks and bends in the polymer chain and by the quantum-assisted transport of the delocalized excitation. Very importantly, there was in both cases a stronger ultrafast depolarization with excitation at 400 nm compared to 500 nm. This provides evidence that absorption with more excess energy, higher into the energy bands, gives rise to a higher initial delocalization and to more loss of anisotropy during the self-localization.

We have recently discussed the implications of the ultrafast relaxation processes in pristine PCDTBT on the photoinduced charge separation in PCDTBT:$PC_{70}BM$ bulk heterojunction blends.[63] Judging from their similar time scales, the charge separation occurs during the initial self-localization, before the photoexcitation becomes bound in a singlet exciton. We suggested that the high initial mobility of the electrons and holes directly after the $\pi-\pi^*$ interband transition and their high delocalization, allowing quantum mechanical spatial displacement,[85] could lead to their ultrafast transport to a polymer:fullerene interface and account for the observed ultrafast charge separation rate in BHJ blends. The charge separation in annealed P3HT:PCBM blends also occurs in less than 120 fs,[32] thus in parallel with the self-localization of the photoexcitation in P3HT. A significant distance (∼10 nm) has to be covered by this excitation in <120 fs to reach an interface, since there is experimental evidence that phase separation between the polymer and fullerene is necessary for a well-functioning solar cell.[8] The present experiments provide strong confirmation that the primary photoexcitation, before it self-localizes and becomes an exciton, is highly delocalized in P3HT. This result supports the mechanism for charge separation that we proposed in PCDTBT and allows generalization to P3HT. Note that the ultrafast transport of the delocalized photoexcitation from amorphous

to crystalline regions in pristine P3HT probably occurs by the same mechanism as the transport to a fullerene interface in P3HT:PCBM blends.

Following the ultrafast self-localization, further spectral relaxation occurs with 0.7, 6.0, and 41 ps time constants in solution, at either excitation wavelength. In the film, the relaxation is slightly slower with 400 nm excitation (0.6, ps, 5.3 and 60 ps) compared to 500 nm excitation (0.3, 2.5, and 40 ps), because more excess energy is initially brought to the system. We ascribe the relaxation that occurs in ~1 ps to singlet exciton formation, which involves thermalization of the photoexcited electron and hole to the band edges, as well as their spatial recombination and Coulomb binding. Exciton formation is observed as an early spectral rise of the emission spectrum in solution and film. For P3HT in solution, this rise starts at higher energy when the polymer is excited higher into the energy bands at 400 nm, confirming our assignment. The relatively slow exciton formation represents further evidence that <120 fs charge separation in P3HT:PCBM blends occurs before the primary photoexcitation becomes a bound exciton. Once the exciton is formed, it can hop to localized states with lower energy that exist as a consequence of disorder. All three time constants of the observed spectral relaxation and concomitant depolarization have a contribution from exciton hopping. This Förster-type transport of the exciton to shorter polymer segments leads to a fast decrease of the emission intensity on the high energy side of the spectrum by 0.5−1 ps one-step hops. Then cascading and decelerating energy migration leads to the observed slightly progressive red-shift of the emission spectrum. The exciton hopping is clearly slower than the <120 fs charge separation in annealed P3HT:PCBM films and therefore cannot account for the ultrafast transport of the excitation to an interface nor for the <200 fs transport of the photoexcitation from amorphous to crystalline regions in pristine P3HT film.

The main spectral changes that we observed are, however, related to the vibronic structure of the emission. In solution, the 0−1 sideband is more forbidden at early time delays. It grows with the 6.0 and 41 ps time constants due to slow planarization of the entire polymer backbone which increases the 0−1 oscillator strength and also turns the emission dipole (depolarization). This slow torsional relaxation is related to low frequency vibrations and possibly thermally activated. In the P3HT film, both the 0−0 and 0−1 bands are present at 0.2 ps, but the 0−0 band has a much higher relative intensity, although this transition is symmetry forbidden in perfect H-aggregates. This band decays to a much smaller relative intensity with the three time constants of the spectral relaxation and depolarization, which we mainly ascribe to slow torsional relaxation of the polymer backbone. The planarization affects the Huang−Rhys factor by changing the equilibrium position of the Franck−Condon active C═C stretching vibration, reduces disorder-induced 0−0 emission, and mediates vibrational relaxation of hot aggregates with allowed emission in the 0−0 spectral region. The fastest subpicosecond decay of the 0−0 band could also be caused by intraband thermalization to the band edges.

Finally, a relaxed intrachain exciton is formed in solution, and a relaxed interchain exciton is formed in the film on the 100−200 ps time scale. These species gives rise to the steady-state emission spectrum, but they clearly appear too slowly to be involved in the charge separation occurring in P3HT:PCBM blends. Significant polarization anisotropy is conserved in the intrachain exciton in solution, which can only decay on the nanosecond time scale by large-scale polymer reorientation. The remaining anisotropy in the film decays faster (with 400 ps), as the interchain excitons have the possibility to hop to neighboring polymer chains. Both intra- and interchain excitons decay on the 500 ps time scale, by intersystem crossing to the triplet state in solution and by nonradiative recombination in the film. The fluorescence quantum yield is nevertheless much lower for the film due to the interchain character of the emission from H-aggregates and to the loss of the initial excitation to polaron species.

AUTHOR INFORMATION

Corresponding Author

*E-mail: ajhe1@physics.ucsb.edu.

ACKNOWLEDGMENT

N.B. thanks the Swiss National Science Foundation for Fellowship support (fellowship for prospective researchers PBGEP2-125859). S.C. thanks the UCSB Center for Energy Efficient Materials, an Energy Frontier Research Center, funded by the U.S. Department of Energy under award number DE-SC0001009. We thank the Department of Energy (BES-DOE-ER46535; A. Kini, Program Officer) for research support. A.J.H. thanks Dr. Daniel Moses for stimulating discussions regarding photoinduced charge transfer in BHJ blends.

REFERENCES

(1) Heeger, A. J. *Chem. Soc. Rev.* **2010**, *39*, 2354–2371.

(2) Skotheim, T. A.; Reynolds, J. R.; Eds. Conjugated polymers, theory, synthesis, properties, and characterization. *Handbook of Conducting Polymers*, 3rd ed.; CRC Press, Taylor & Francis Group: Boca Raton, FL, 2007.

(3) Dennler, G.; Sariciftci, N. S.; Brabec, C. J. *Semiconducting Polymers*, 2nd ed.; Wiley: New York, 2007; Vol. 2, pp 455−530.

(4) Malliaras, G.; Friend, R. *Phys. Today* **2005**, *58*, 53–58.

(5) Forrest, S. R. *Nature* **2004**, *428*, 911–918.

(6) Thompson, B. C.; Frechet, J. M. J. *Angew. Chem., Int. Ed.* **2008**, *47*, 58–77.

(7) Kim, J. Y.; Lee, K.; Coates, N. E.; Moses, D.; Nguyen, T.-Q.; Dante, M.; Heeger, A. J. *Science (Washington, D.C.)* **2007**, *317*, 222–225.

(8) Ma, W.; Yang, C.; Gong, X.; Lee, K.; Heeger, A. J. *Adv. Funct. Mater.* **2005**, *15*, 1617–1622.

(9) Brabec, C. J. *Sol. Energy Mater. Sol. Cells* **2004**, *83*, 273–292.

(10) Brabec, C. J.; Sariciftci, N. S.; Hummelen, J. C. *Adv. Funct. Mater.* **2001**, *11*, 15–26.

(11) Shaheen, S. E.; Brabec, C. J.; Sariciftci, N. S.; Padinger, F.; Fromherz, T.; Hummelen, J. C. *Appl. Phys. Lett.* **2001**, *78*, 841–843.

(12) Yu, G.; Gao, J.; Hummelen, J. C.; Wudl, F.; Heeger, A. J. *Science (Washington, D.C.)* **1995**, *270*, 1789–1791.

(13) Kim, J. Y.; Kim, S. H.; Lee, H. H.; Lee, K.; Ma, W. L.; Gong, X.; Heeger, A. J. *Adv. Mater. (Weinheim, Ger.)* **2006**, *18*, 572–576.

(14) Reyes-Reyes, M.; Kim, K.; Carroll, D. L. *Appl. Phys. Lett.* **2005**, *87*, 083506.

(15) Li, G.; Shrotriya, V.; Huang, J. S.; Yao, Y.; Moriarty, T.; Emery, K.; Yang, Y. *Nat. Mater.* **2005**, *4*, 864–868.

(16) Xie, Y.; Li, Y.; Xiao, L.; Qiao, Q.; Dhakal, R.; Zhang, Z.; Gong, Q.; Galipeau, D.; Yan, X. *J. Phys. Chem. C* **2010**, *114*, 14590–14600.

(17) Parkinson, P.; Muller, C.; Stingelin, N.; Johnston, M. B.; Herz, L. M. *J. Phys. Chem. Lett.* **2010**, *1*, 2788–2792.

(18) Marsh, R. A.; Hodgkiss, J. M.; Albert-Seifried, S.; Friend, R. H. *Nano Lett.* **2010**, *10*, 923–930.

(19) Lee, Y. H.; Yabushita, A.; Hsu, C. S.; Yang, S. H.; Iwakura, I.; Luo, C. W.; Wu, K. H.; Kobayashi, T. *Chem. Phys. Lett.* **2010**, *498*, 71–76.

(20) Guo, J. M.; Ohkita, H.; Benten, H.; Ito, S. *J. Am. Chem. Soc.* **2010**, *132*, 6154–6164.
(21) Cook, S.; Liyuan, H.; Furube, A.; Katoh, R. *J. Phys. Chem. C* **2010**, *114*, 10962–10968.
(22) Cook, S.; Katoh, R.; Furube, A. *J. Nanoelectron. Optoelectron.* **2010**, *5*, 115–119.
(23) Trotzky, S.; Hoyer, T.; Tuszynski, W.; Lienau, C.; Parisi, J. *J. Phys. D. Appl. Phys.* **2009**, *42*, 055105.
(24) Ruseckas, A.; Shaw, P. E.; Samuel, I. D. W. *Dalton Trans.* **2009**, 10040–10043.
(25) Piris, J.; Dykstra, T. E.; Bakulin, A. A.; van Loosdrecht, P. H. M.; Knulst, W.; Trinh, M. T.; Schins, J. M.; Siebbeles, L. D. A. *J. Phys. Chem. C* **2009**, *113*, 14500–14506.
(26) Guo, J. M.; Ohkita, H.; Benten, H.; Ito, S. *J. Am. Chem. Soc.* **2009**, *131*, 16869–16880.
(27) Cook, S.; Katoh, R.; Furube, A. *J. Phys. Chem. C* **2009**, *113*, 2547–2552.
(28) Clarke, T. M.; Jamieson, F. C.; Durrant, J. R. *J. Phys. Chem. C* **2009**, *113*, 20934–20941.
(29) Clark, J.; Chang, J.-F.; Spano, F. C.; Friend, R. H.; Silva, C. *Appl. Phys. Lett.* **2009**, *94*, 163306.
(30) Wells, N. P.; Blank, D. A. *Phys. Rev. Lett.* **2008**, *100*, 086403.
(31) Parkinson, P.; Lloyd-Hughes, J.; Johnston, M. B.; Herz, L. M. *Phys. Rev. B* **2008**, *78*, 115321.
(32) Hwang, I. W.; Moses, D.; Heeger, A. J. *J. Phys. Chem. C* **2008**, *112*, 4350–4354.
(33) Ferguson, A. J.; Kopidakis, N.; Shaheen, S. E.; Rumbles, G. *J. Phys. Chem. C* **2008**, *112*, 9865–9871.
(34) Du, J.; Wang, Z.; Feng, W.; Yoshino, K.; Kobayashi, T. *Phys. Rev. B: Condens. Matter Mater. Phys.* **2008**, *77*, 195205.
(35) Cunningham, P. D.; Hayden, L. M. *J. Phys. Chem. C* **2008**, *112*, 7928–7935.
(36) Cook, S.; Furube, A.; Katoh, R. *Energy Environ. Sci.* **2008**, *1*, 294–299.
(37) Wells, N. P.; Boudouris, B. W.; Hillmyer, M. A.; Blank, D. A. *J. Phys. Chem. C* **2007**, *111*, 15404–15414.
(38) Sheng, C. X.; Tong, M.; Singh, S.; Vardeny, Z. V. *Phys. Rev. B* **2007**, *75*, 085206.
(39) Janssen, G.; Aguirre, A.; Goovaerts, E.; Vanlaeke, P.; Poortmans, J.; Manca, J. *Eur. Phys. J.: Appl. Phys.* **2007**, *37*, 287–290.
(40) Clark, J.; Silva, C.; Friend, R. H.; Spano, F. C. *Phys. Rev. Lett.* **2007**, *98*, 206406.
(41) Saeki, A.; Seki, S.; Sunagawa, T.; Ushida, K.; Tagawa, S. *Philos. Mag.* **2006**, *86*, 1261–1276.
(42) Spano, F. C. *Chem. Phys.* **2006**, *325*, 22–35.
(43) Spano, F. C. *J. Chem. Phys.* **2005**, *122*, 234701.
(44) Kobayashi, T.; Hamazaki, J.; Kunugita, H.; Ema, K.; Endo, T.; Rikukawa, M.; Sanui, K. *Phys. Rev. B* **2003**, *67*, 205214.
(45) Brown, P. J.; Thomas, D. S.; Kohler, A.; Wilson, J. S.; Kim, J. S.; Ramsdale, C. M.; Sirringhaus, H.; Friend, R. H. *Phys. Rev. B* **2003**, *67*, 064203.
(46) Jiang, X. M.; Osterbacka, R.; Korovyanko, O.; An, C. P.; Horovitz, B.; Janssen, R. A. J.; Vardeny, Z. V. *Adv. Funct. Mater.* **2002**, *12*, 587–597.
(47) Westerling, M.; Osterbacka, R.; Stubb, H. *Synth. Met.* **2001**, *119*, 623–624.
(48) Ruseckas, A.; Namdas, E. B.; Theander, M.; Svensson, M.; Yartsev, A.; Zigmantas, D.; Andersson, M. R.; Inganas, O.; Sundstrom, V. *J. Photochem. Photobiol. A* **2001**, *144*, 3–12.
(49) Osterbacka, R.; An, C. P.; Jiang, X. M.; Vardeny, Z. V. *Synth. Met.* **2001**, *116*, 317–320.
(50) Korovyanko, O. J.; Osterbacka, R.; Jiang, X. M.; Vardeny, Z. V.; Janssen, R. A. J. *Phys. Rev. B: Condens. Matter Mater. Phys.* **2001**, *64*, 235122.
(51) Osterbacka, R.; An, C. P.; Jiang, X. M.; Vardeny, Z. V. *Science (Washington, D.C.)* **2000**, *287*, 839–842.
(52) Shiga, T.; Ikawa, T.; Okada, A. *J. Appl. Polym. Sci.* **1998**, *67*, 259–266.
(53) Samuel, I. D. W.; Magnani, L.; Rumbles, G.; Murray, K.; Stone, B. M.; Moratti, S. C.; Holmes, A. B. *Proc. SPIE-Int. Soc. Opt. Eng.* **1997**, *3145*, 163–170.
(54) Magnani, L.; Rumbles, G.; Samuel, I. D. W.; Murray, K.; Moratti, S. C.; Holmes, A. B.; Friend, R. H. *Synth. Met.* **1997**, *84*, 899–900.
(55) Kraabel, B.; Moses, D.; Heeger, A. J. *J. Chem. Phys.* **1995**, *103*, 5102–5108.
(56) Hotta, S.; Rughooputh, S. D. D. V.; Heeger, A. J.; Wudl, F. *Macromolecules* **1987**, *20*, 212–215.
(57) Scheblykin, I. G.; Yartsev, A.; Pullerits, T.; Gulbinas, V.; Sundstrom, V. *J. Phys. Chem. B* **2007**, *111*, 6303–6321.
(58) Barford, W. *Electronic and Optical Properties of Conjugated Polymers*; Oxford University Press: Oxford, UK, 2005.
(59) Lanzani, G.; Cerullo, G.; Polli, D.; Gambetta, A.; Zavelani-Rossi, M.; Gadermaier, C. *Phys. Status Solidi A* **2004**, *201*, 1116–1131.
(60) Sariciftci, N. S. *Primary Photoexcitations in Conjugated Polymers: Molecular Exciton versus Semiconductor Band Model*; World Scientific: Singapore, 1997.
(61) Sirringhaus, H.; Brown, P. J.; Friend, R. H.; Nielsen, M. M.; Bechgaard, K.; Langeveld-Voss, B. M. W.; Spiering, A. J. H.; Janssen, R. A. J.; Meijer, E. W.; Herwig, P.; de Leeuw, D. M. *Nature* **1999**, *401*, 685–688.
(62) Heeger, A. J.; Sariciftci, N. S.; Namdas, E. B. *Semiconducting and Metallic Polymers*; Oxford University Press: Oxford, UK, 2010.
(63) Banerji, N.; Cowan, S.; Leclerc, M.; Vauthey, E.; Heeger, A. J. *J. Am. Chem. Soc.* **2010**, *132*, 17459.
(64) Morandeira, A.; Engeli, L.; Vauthey, E. *J. Phys. Chem. A* **2002**, *106*, 4833–4837.
(65) Furstenberg, A.; Vauthey, E. *J. Phys. Chem. B* **2007**, *111*, 12610–12620.
(66) Moses, D.; Schmechel, R.; Heeger, A. J. *Synth. Met.* **2003**, *139*, 807–810.
(67) Moses, D.; Wang, J.; Heeger, A. J.; Kirova, N.; Brazovski, S. *Proc. Natl. Acad. Sci. U. S. A.* **2001**, *98*, 13496–13500.
(68) Miranda, P. B.; Moses, D.; Heeger, A. J. *Synth. Met.* **2001**, *119*, 619–620.
(69) Miranda, P. B.; Moses, D.; Heeger, A. J. *Phys. Rev. B* **2001**, *6408*, 081201.
(70) Moses, D.; Dogariu, A.; Heeger, A. J. *Phys. Rev. B* **2000**, *61*, 9373–9379.
(71) Moses, D.; Soci, C.; Miranda, P.; Heeger, A. J. *Chem. Phys. Lett.* **2001**, *350*, 531–536.
(72) Hagler, T. W.; Pakbaz, K.; Heeger, A. J. *Phys. Rev. B* **1995**, *51*, 14199–14206.
(73) Hagler, T. W.; Pakbaz, K.; Heeger, A. J. *Phys. Rev. B* **1994**, *49*, 10968–10975.
(74) Hagler, T. W.; Pakbaz, K.; Voss, K. F.; Heeger, A. J. *Phys. Rev. B* **1991**, *44*, 8652–8666.
(75) Hagler, T. W.; Pakbaz, K.; Moulton, J.; Wudl, F.; Smith, P.; Heeger, A. J. *Polym. Commun.* **1991**, *32*, 339–342.
(76) Duvanel, G.; Grilj, J.; Schuwey, A.; Gossauer, A.; Vauthey, E. *Photochem. Photobiol. Sci.* **2007**, *6*, 956–963.
(77) Spano, F. C.; Clark, J.; Silva, C.; Friend, R. H. *J. Chem. Phys.* **2009**, *130*, 074904.
(78) Su, W. P.; Schrieffer, J. R. *Proc. Natl. Acad. Sci. U. S. A.* **1980**, *77*, 5626–5629.
(79) Ruseckas, A.; Wood, P.; Samuel, I. D. W.; Webster, G. R.; Mitchell, W. J.; Burn, P. L.; Sundstrom, V. *Phys. Rev. B* **2005**, *72*, 115214.
(80) Yang, X. J.; Dykstra, T. E.; Scholes, G. D. *Phys. Rev. B* **2005**, *71*, 045203.
(81) Dykstra, T. E.; Kovalevskij, V.; Yang, X. J.; Scholes, G. D. *Chem. Phys.* **2005**, *318*, 21–32.
(82) Milota, F.; Sperling, J.; Tortschanoff, A.; Szocs, V.; Kuna, L.; Kauffmann, H. F. *J. Lumin.* **2004**, *108*, 205–209.
(83) Grage, M. M. L.; Zaushitsyn, Y.; Yartsev, A.; Chachisvilis, M.; Sundstrom, V.; Pullerits, T. *Phys. Rev. B* **2003**, *67*, 205207.
(84) Grage, M. M. L.; Pullerits, T.; Ruseckas, A.; Theander, M.; Inganas, O.; Sundstrom, V. *Chem. Phys. Lett.* **2001**, *339*, 96–102.

(85) Collini, E.; Scholes, G. D. *Science (Washington, D.C.)* **2009**, *323*, 369–373.
(86) Shaw, P. E.; Ruseckas, A.; Samuel, I. D. W. *Adv. Mater.* **2008**, *20*, 3516–3520.
(87) Pina, J.; de Melo, J. S.; Burrows, H. D.; Bunnagel, T. W.; Dolfen, D.; Kudla, C. J.; Scherf, U. *J. Phys. Chem. B* **2009**, *113*, 15928–15936.
(88) Westenhoff, S.; Beenken, W. J. D.; Friend, R. H.; Greenham, N. C.; Yartsev, A.; Sundstrom, V. *Phys. Rev. Lett.* **2006**, *97*, 166804.
(89) Sperling, J.; Milota, F.; Kauffmann, H. F. *Opt. Spectrosc.* **2005**, *98*, 729–739.
(90) Sperling, J.; Milota, F.; Tortschanoff, A.; Warmuth, C.; Mollay, B.; Bassler, H.; Kauffmann, H. F. *J. Chem. Phys.* **2002**, *117*, 10877–10887.
(91) Kennedy, S. P.; Garro, N.; Phillips, R. T. *Phys. Rev. B* **2001**, *6411*, 115206.
(92) Meskers, S. C. J.; Hubner, J.; Oestreich, M.; Bassler, H. *J. Phys. Chem. B* **2001**, *105*, 9139–9149.
(93) Warmuth, C.; Tortschanoff, A.; Brunner, K.; Mollay, B.; Kauffmann, H. F. *J. Lumin.* **1998**, *76−7*, 498–501.
(94) Hayes, G. R.; Samuel, I. D. W.; Phillips, R. T. *Synth. Met.* **1997**, *84*, 889–890.
(95) Hayes, G. R.; Samuel, I. D. W.; Phillips, R. T. *Phys. Rev. B* **1995**, *52*, 11569–11572.
(96) Kersting, R.; Mollay, B.; Rusch, M.; Wenisch, J.; Leising, G.; Kauffmann, H. F. *J. Chem. Phys.* **1997**, *106*, 2850–2864.
(97) Kersting, R.; Lemmer, U.; Mahrt, R. F.; Leo, K.; Kurz, H.; Bassler, H.; Gobel, E. O. *Phys. Rev. Lett.* **1993**, *70*, 3820–3823.
(98) Karabunarliev, S.; Baumgarten, M.; Bittner, E. R.; Mullen, K. *J. Chem. Phys.* **2000**, *113*, 11372–11381.
(99) Sluch, M. I.; Godt, A.; Bunz, U. H. F.; Berg, M. A. *J. Am. Chem. Soc.* **2001**, *123*, 6447–6448.
(100) Di Paolo, R. E.; de Melo, J. S.; Pina, J.; Burrows, H. D.; Morgado, J.; Macanita, A. L. *ChemPhysChem* **2007**, *8*, 2657–2664.
(101) Hintschich, S. I.; Dias, F. B.; Monkman, A. P. *Phys. Rev. B* **2006**, *74*, 045210.
(102) Bittner, E. R.; Karabunarliev, S.; Herz, L. M. *J. Chem. Phys.* **2007**, *126*, 191102.